2016 IEEE/RSJ International Conference on Intelligent Robots and Systems (IROS)
Daejeon Convention Center
October 9-14, 2016, Daejeon, Korea

Hybrid Force/Velocity Control for Physical Human-Robot Collaboration Tasks

Emanuele Magrini Alessandro De Luca

Abstract— **During human-robot collaboration tasks, we may physically touch the robot at a generic location and engage an intentional exchange of forces while realizing coordinated motion of the common contact point. In order to control the relative motion and the exchanged contact forces, the latter need to be estimated without using any local force sensing device. Building upon our recent works, we generalize the classical hybrid force/velocity control design to this situation, handling complementary quantities along the directions of a suitable contact task frame in a dynamically decoupled way. The contact force is estimated online using our residual method together with an external sensor to localize the contact point, and the time-varying contact task frame is obtained analytically from this estimate. Experimental results are presented for a KUKA LWR4 robot using a Kinect sensor.**

I. Introduction

Recent progresses dealing with physical Human-Robot Interaction (pHRI) have covered in an integrated way mechanical, actuation, sensing, planning and control issues, with the goal of increasing safety and dependability of robotic systems [1]. Within the European FP7 research project SAPHARI [2], we have originally proposed a control architecture devoted to pHRI, which is organized in three nested functional layers addressing, respectively, human-robot safety, coexistence, and collaboration [3]. Upper layers will prescribe only robot reactive behaviors that are consistent with the objectives and constraints of lower layers. Interestingly enough, the layers of the proposed control architecture can also be mapped one-to-one to the requirements of safety standards for collaborative robots [4], [5].

This general framework has allowed to integrate previous or newly developed research results, using the KUKA LWR as the target manipulator and a ROS environment. In particular, collision detection, isolation, and reflex reaction based on the residuals [6]–[8] have been implemented in the *safety* layer, whereas the monitoring of the shared workspace by external sensors (cameras, RGB-D, laser), a robust and efficient method for on-line human-robot distance/separation evaluation, and the related collision avoidance algorithms [9], [10] are now part of the *coexistence* layer.

The top control layer is devoted to handling both contactless human-robot coordination and, most importantly, physical *collaboration* tasks, in which a continuous and intentional contact should take place with a controlled exchange of forces/torques, as activated by multimodal communication such as voice, gestures, or touch [11], [12]. In order for the robot to execute a wider range of collaborative activities, contacts may not be limited to a designated end-effector tool, but rather whole-arm manipulation conditions should be considered. This raises the additional issue of reconstructing the exchanged forces at generic contact points along the robot structure, either by measuring them (e.g., placing patches of conformable tactile skin in different locations [13]) or by estimating them in an indirect way, possibly combining model-based methods with other less invasive external sensors. In [14], a first example of a method that estimates contact forces occurring at generic points (a priori unknown) on the robot arm was given. This was obtained by a *virtual* force sensor, which combines the proprioceptive information of the residual signals with the localization of the contact location provided by a Kinect.

Once an estimated contact force is available, this can be exploited for control purposes. One simple use is the variable joint space impedance realized in this way by [15]. We have pursued instead a control design that focuses on the regulation of the robot behavior at or around the current *contact point*, where the exchange of forces is taking place. In this respect, we were able to generalize standard approaches such as *admittance control* [14], which relates the contact velocity to the estimated force, disregarding the robot dynamic model, as well as *impedance control* (with of without changing the apparent inertia at the contact) and direct *force control* [16]. In the latter case, a task incompatibility issue was found, namely the impossibility for the robot to regulate a desired non-zero value of the contact force in a Cartesian direction along which the human is not pushing at all. Further details can be found in [17].

In this paper, we add another element to the portfolio of generalized control laws developed so far for physical human-robot collaboration, namely *hybrid force/velocity control* at the contact point, realized using just the contact force estimated by the virtual sensing method in [14]. In fact, the task incompatibility phenomenon mentioned above for the direct force control scheme is reminiscent of the classical concept of *task frame* [18], which led more than two decades ago to the decoupled design of hybrid force-velocity controllers, first at the kineto-static level [19], [20], and then correctly including the full robot dynamics [21]–[23]. By taking this perspective, we shall see how is it possible to regulate the intensity of the contact force along the instantaneous direction of approach to the robot chosen by the human, while nicely tracking a desired velocity profile

The authors are with the Dipartimento di Ingegneria Informatica, Automatica e Gestionale, Sapienza Università di Roma, Via Ariosto 25, 00185 Roma, Italy ({magrini,deluca}@diag.uniroma1.it). This work is supported by the European Commission, within the H2020 projects FoF-637080 SYMPLEXITY (www.symplexity.eu) and ICT-645097 COMANOID (www.comanoid.eu).

in the orthogonal plane to this direction. For the ease of presentation, we will consider here only point-wise contacts (no exchanged moments).

With respect to other existing schemes for handling human-robot interaction, the proposed hybrid force/velocity controller is best suited for applications that require simultaneous collaboration both in motion and force. One possible example is the collaborative transport of a payload along a desired trajectory (motion task). The carried object is not necessarily held at the end-effector level, and needs thus a net pushing force jointly applied at the contact by the human hand and the robot body to be kept firmly (force task). For this form of whole-body collaborative manipulation, an impedance scheme would not be fully appropriate. In fact, a force regulation loop is not explicitly present and setting a desired force at the contact is impossible. Moreover, compliance along the force controlled direction requires a zero-reference position which is not known a priori, but rather only implicitly defined online by the user.

The paper is organized as follows. Section II briefly recalls the background material used in the paper, including the contact force estimation method in [14]. Section III details how to recover instantaneously a contact task frame implicitly defined by the user during the interaction, starting from the estimated contact force. The generalization of hybrid force/velocity control design to handle contact situations occurring at a generic point of a multi-dof manipulator is presented in Sec. IV. Section V reports on experimental results obtained with the proposed method during physical human-robot collaboration with a KUKA LWR4 robot and using a Kinect sensor.

II. Preliminaries

Consider a robot manipulator with n joints and generalized coordinates $\boldsymbol{q} \in \mathbb{R}^n$, performing at a contact point $\boldsymbol{x}_c \in \mathbb{R}^3$ on its structure a force/motion interaction task (with a human). The Cartesian velocity of the contact point is given by $\dot{\boldsymbol{x}}_c = \boldsymbol{J}_c(\boldsymbol{q})\dot{\boldsymbol{q}}$ and its acceleration is

$$\ddot{\boldsymbol{x}}_c = \boldsymbol{J}_c(\boldsymbol{q})\ddot{\boldsymbol{q}} + \dot{\boldsymbol{J}}_c(\boldsymbol{q})\dot{\boldsymbol{q}}, \tag{1}$$

where $\boldsymbol{J}_c$ is the $3 \times n$ *contact Jacobian* matrix. Note that when the contact point is located on the robot link k, with $k \in \{1, \ldots, n\}$, the last $n-k$ columns of $\boldsymbol{J}_c$ will be identically zero. As long as $k > 3$, the robot will be redundant with respect to the given interaction task.

At a robot state $(\boldsymbol{q}, \dot{\boldsymbol{q}})$, all joint accelerations associated to a desired acceleration $\ddot{\boldsymbol{x}}_c$ of the contact point can be written as

$$\ddot{\boldsymbol{q}} = \boldsymbol{J}^{\#}_{c,W}(\ddot{\boldsymbol{x}}_c - \dot{\boldsymbol{J}}_c\dot{\boldsymbol{q}}) + \boldsymbol{P}_{c,W}\,\ddot{\boldsymbol{q}}_0, \tag{2}$$

where $\boldsymbol{J}^{\#}_{c,W}$ is a $n \times 3$ weighted (with $\boldsymbol{W} > 0$) pseudoinverse of the contact Jacobian, $\ddot{\boldsymbol{q}}_0 \in \mathbb{R}^n$ is an arbitrary joint acceleration, and $\boldsymbol{P}_{c,W} = \boldsymbol{I} - \boldsymbol{J}^{\#}_{c,W}\boldsymbol{J}_c$ is a projector in the null space of $\boldsymbol{J}_c$.

With reference to Fig. 1, let O_t–$\boldsymbol{x}_t\boldsymbol{y}_t\boldsymbol{z}_t$ be a (contact) task frame with origin O_t coincident with the contact point $\boldsymbol{x}_c$ and $\boldsymbol{z}_t$ unitary vector aligned with the external contact force $\boldsymbol{F}_c \in \mathbb{R}^3$ acting on that point. The velocity $\dot{\boldsymbol{x}}_c$ is related to its expression ${}^t\dot{\boldsymbol{x}}_c$ in the contact task frame by

$$\dot{\boldsymbol{x}}_c = \boldsymbol{R}_t(\boldsymbol{z}_t)\,{}^t\dot{\boldsymbol{x}}_c,$$

where $\boldsymbol{R}_t$ is the rotation matrix giving the (time-varying) orientation of the contact task frame. Similarly, the associated acceleration vector can be rewritten as

$$\ddot{\boldsymbol{x}}_c = \boldsymbol{R}_t\,{}^t\ddot{\boldsymbol{x}}_c + \dot{\boldsymbol{R}}_t\,{}^t\dot{\boldsymbol{x}}_c, \tag{3}$$

where $\dot{\boldsymbol{R}}_t$ is the time derivative of the rotation matrix $\boldsymbol{R}_t$. Substituting (3) in (2) yields

$$\ddot{\boldsymbol{q}} = \boldsymbol{J}^{\#}_{c,W}(\boldsymbol{R}_t\,{}^t\ddot{\boldsymbol{x}}_c + \dot{\boldsymbol{R}}_t\,{}^t\dot{\boldsymbol{x}}_c - \dot{\boldsymbol{J}}_c\dot{\boldsymbol{q}}) + \boldsymbol{P}_{c,W}\ddot{\boldsymbol{q}}_0. \tag{4}$$

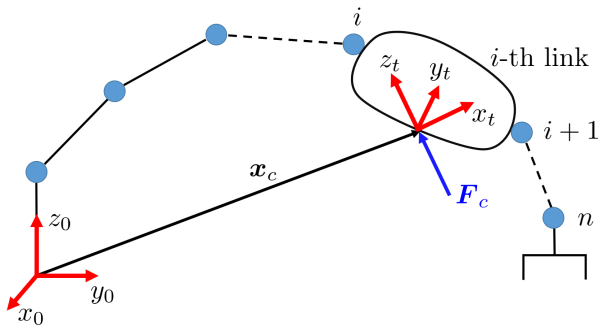

Fig. 1. A contact force $\boldsymbol{F}_c$ acting on link i, with its associated task frame attached to the contact point $\boldsymbol{x}_c$.

Finally, the dynamic model of a rigid robot in contact with the environment at point $\boldsymbol{x}_c$ is given by

$$\boldsymbol{M}(\boldsymbol{q})\ddot{\boldsymbol{q}} + \boldsymbol{n}(\boldsymbol{q}.\dot{\boldsymbol{q}}) = \boldsymbol{\tau} + \boldsymbol{J}_c^T(\boldsymbol{q})\boldsymbol{F}_c, \tag{5}$$

where $\boldsymbol{M}(\boldsymbol{q})$ is the inertia matrix, $\boldsymbol{n}(\boldsymbol{q}, \dot{\boldsymbol{q}}) = \boldsymbol{C}(\boldsymbol{q}, \dot{\boldsymbol{q}})\dot{\boldsymbol{q}} + \boldsymbol{g}(\boldsymbol{q})$ includes Coriolis, centrifugal (factorized by the Christoffel symbols) and gravitational terms, $\boldsymbol{\tau} \in \mathbb{R}^n$ is the control torque, and $\boldsymbol{\tau}_c = \boldsymbol{J}_c^T(\boldsymbol{q})\boldsymbol{F}_c$ is the joint torque resulting from the interaction force $\boldsymbol{F}_c$.

In the framework of operational space control [21], it has been shown that using the inertia-weighted pseudoinverse in (2), i.e., setting $\boldsymbol{W} = \boldsymbol{M}(\boldsymbol{q})$, will guarantee consistency of the transformation of task forces in the robot dynamics. Provided $\boldsymbol{J}_c$ is full rank, the inertia-weighted pseudoinverse of the contact Jacobian takes the form

$$\boldsymbol{J}^{\#}_{c,\boldsymbol{M}} = \boldsymbol{M}^{-1}\boldsymbol{J}_c^T(\boldsymbol{J}_c\boldsymbol{M}^{-1}\boldsymbol{J}_c^T)^{-1}. \tag{6}$$

In the following, to simplify notation, each pseudoinverse $\boldsymbol{J}_c^{\#}$ is to be intended as the inertia-weighted one given by (6).

A. Contact force estimation

For a robot with dynamics (5), the residual vector $\boldsymbol{r} \in \mathbb{R}^n$ is defined as [6]

$$\boldsymbol{r}(t) = \boldsymbol{K}_I\left(\boldsymbol{p} - \int_0^t \left(\boldsymbol{\tau} + \boldsymbol{C}^T(\boldsymbol{q}, \dot{\boldsymbol{q}})\dot{\boldsymbol{q}} - \boldsymbol{g}(\boldsymbol{q}) + \boldsymbol{r}\right) ds\right), \tag{7}$$

where $\boldsymbol{p} = \boldsymbol{M}(\boldsymbol{q})\dot{\boldsymbol{q}}$ is the generalized momentum of the robot and $\boldsymbol{K}_I > 0$ is a diagonal gain matrix. The dynamic evolution of $\boldsymbol{r}$ has the stable, first-order low-pass filter structure

$$\dot{\boldsymbol{r}} = \boldsymbol{K}_I(\boldsymbol{\tau}_c - \boldsymbol{r}).$$

Therefore, for sufficiently large gains, we can assume that

$$\boldsymbol{r} \simeq \boldsymbol{\tau}_c = \boldsymbol{J}_c^T(\boldsymbol{q})\boldsymbol{F}_c. \tag{8}$$

Equation (8) forms the basis for the estimations of the unknown contact force $\boldsymbol{F}_c \in \mathbb{R}^3$. Using external sensing, the contact point $\boldsymbol{x}_c$ can be localized, and thus the associated contact Jacobian $\boldsymbol{J}_c$ can be computed. Depending on which link in the kinematic chain is involved in the contact, (8) may consist of a square, under-, or over-determined linear system. In any case, the contact force is estimated by pseudoinversion as

$$\widehat{\boldsymbol{F}}_c = \left(\boldsymbol{J}_c^T(\boldsymbol{q})\right)^{\#}\boldsymbol{r}. \tag{9}$$

Indeed, the estimate $\widehat{\boldsymbol{F}}_c$ will be limited only to those components of $\boldsymbol{F}_c$ that can be detected by the residual $\boldsymbol{r}$, namely those contact forces that do not belong to the null space $\mathcal{N}(\boldsymbol{J}_c^T(\boldsymbol{q}))$. For further details and for the analysis of cases when the contact Jacobian is not full rank, see [17].

B. Objective of the controller

After entering a collaboration mode (e.g., through a human gesture or a voice command), as soon as a contact along the robot structure is established and detected, the control law should realize the following robot behavior in a hybrid task:

1) keep the human-robot physical contact at the point where the first contact was detected; this point is specified by a constant position vector $\boldsymbol{p}_c \in \mathbb{R}^3$ defined in the frame attached to the link that undergoes contact;
2) apply a desired force at the contact point along the instantaneous direction of the estimated contact force $\widehat{\boldsymbol{F}}_c \in \mathbb{R}^3$, with intensity $F_d > 0$ (force control task);
3) move the contact point with desired velocity $\boldsymbol{\nu}_d \in \mathbb{R}^2$ defined in the normal plane to the instantaneously estimated contact force (velocity control task).

The values F_d and $\boldsymbol{\nu}_d$ may also be function of time. The collaboration mode will be ended by another user-defined command. In our experiments, the human applies a sudden extra push at the contact and then removes the hand, while the robot stops.

III. Contact Task Frame

In order to extend at the contact level a hybrid force/velocity control law, we need to determine instantaneously the orientation of the contact task frame $O_t{-}\boldsymbol{x}_t\boldsymbol{y}_t\boldsymbol{z}_t$ in which the description of the interaction task is made easy. This task frame is obtained from the world reference frame $O_0{-}\boldsymbol{x}_0\boldsymbol{y}_0\boldsymbol{z}_0$ by a rotation matrix $\boldsymbol{R}_t$ such that $\boldsymbol{z}_t$ is aligned with the contact force $\boldsymbol{F}_c$. Let $\boldsymbol{R}_t$ be defined as

$$\boldsymbol{R}_t = \begin{bmatrix} \boldsymbol{u} & \boldsymbol{v} & \boldsymbol{w} \end{bmatrix} = \begin{bmatrix} \boldsymbol{u} & \boldsymbol{v} & \dfrac{\widehat{\boldsymbol{F}}_c}{\|\widehat{\boldsymbol{F}}_c\|}, \end{bmatrix}, \tag{10}$$

where $\boldsymbol{u}$, $\boldsymbol{v}$, and $\boldsymbol{w}$ are three orthonormal unit vectors, with $\boldsymbol{w}$ oriented as the normalized estimate of the force vector $\widehat{\boldsymbol{F}}_c$,

$$\boldsymbol{w} = \frac{\widehat{\boldsymbol{F}}_c}{\|\widehat{\boldsymbol{F}}_c\|} = \begin{bmatrix} \widehat{F}_{cx} \\ \widehat{F}_{cy} \\ \widehat{F}_{cz} \end{bmatrix} \frac{1}{\|\widehat{\boldsymbol{F}}_c\|}. \tag{11}$$

Indeed, we assume the $\widehat{\boldsymbol{F}}_c \neq \boldsymbol{0}$. Otherwise, there is no (estimated) contact force and thus no contact frame is needed. For the sake of clarity, we shall label the components of $\boldsymbol{w}$ as

$$\boldsymbol{w} = \begin{bmatrix} w_x \\ w_y \\ w_z \end{bmatrix}, \quad \text{with} \quad w_x^2 + w_y^2 + w_z^2 = 1. \tag{12}$$

Without loss of generality, consider the first term w_x of $\boldsymbol{w}$. According to the estimation of contact force $\widehat{\boldsymbol{F}}_c$, three cases may happen:

1) $|w_x| = 1$, i.e., the contact force is applied along the direction of the unit vector $\boldsymbol{x}_0$ of the world frame. Thus, $\boldsymbol{w} = \begin{bmatrix} \pm 1 & 0 & 0 \end{bmatrix}^T$, and the remaining two columns of $\boldsymbol{R}_t$ have to be chosen in such a way that $\det \boldsymbol{R}_t = 1$. The resulting rotation matrix will be
$$\boldsymbol{R}_t = \begin{bmatrix} 0 & 0 & \pm 1 \\ 0 & \mp 1 & 0 \\ 1 & 0 & 0 \end{bmatrix}.$$
2) $0 < |w_x| < 1$, which is the generic case where w_y and/or w_z are non-zero. Let be $\boldsymbol{v}'$ a vector orthogonal to $\boldsymbol{w}$ defined as
$$\boldsymbol{v}' = \begin{bmatrix} \dfrac{1}{w_x} - w_x \\ -w_y \\ -w_z \end{bmatrix}, \quad \text{with} \quad \|\boldsymbol{v}'\| = \frac{\sqrt{1 - w_x^2}}{w_x}.$$
It is easy to verify that $\boldsymbol{w}$ and $\boldsymbol{v}'$ are orthogonal, being $\boldsymbol{w}^T\boldsymbol{v}' = 0$. Normalizing $\boldsymbol{v}'$ we obtain the unit vector
$$\boldsymbol{v} = \frac{\boldsymbol{v}'}{\|\boldsymbol{v}'\|} = \begin{bmatrix} \sqrt{1 - w_x^2} \\ -\dfrac{w_x w_y}{\sqrt{1 - w_x^2}} \\ -\dfrac{w_x w_z}{\sqrt{1 - w_x^2}}. \end{bmatrix}. \tag{13}$$
At this stage, the rotation matrix $\boldsymbol{R}_t$ can be completed by computing the last vector $\boldsymbol{u}$ as
$$\boldsymbol{u} = \boldsymbol{v} \times \boldsymbol{w} = -\boldsymbol{w} \times \boldsymbol{v} = \boldsymbol{S}(-\boldsymbol{w})\boldsymbol{v} = -\boldsymbol{S}(\boldsymbol{w})\boldsymbol{v},$$
with $\boldsymbol{S}(\boldsymbol{w})$ skew-symmetric matrix of $\boldsymbol{w}$. Using (12) and (13), the latter equation becomes
$$\boldsymbol{u} = \begin{bmatrix} 0 & w_z & -w_y \\ -w_z & 0 & w_x \\ w_y & -w_x & 0 \end{bmatrix} \begin{bmatrix} 1 - w_x^2 \\ -w_x w_y \\ -w_x w_z \end{bmatrix} \frac{1}{\sqrt{1 - w_x^2}} = \begin{bmatrix} 0 \\ -w_z \\ w_y \end{bmatrix} \frac{1}{\sqrt{1 - w_x^2}}. \tag{14}$$

From (12), we have $1 - w_x^2 = w_y^2 + w_z^2$ and it easy to check that $\boldsymbol{u}$ is a unit vector. Summarizing and putting together (12), (13), and (14), we obtain the solution as

$$\boldsymbol{R}_t = \begin{bmatrix} 0 & \sqrt{1-w_x^2} & w_x \\ -\dfrac{w_z}{\sqrt{1-w_x^2}} & -\dfrac{w_x w_y}{\sqrt{1-w_x^2}} & w_y \\ \dfrac{w_y}{\sqrt{1-w_x^2}} & -\dfrac{w_x w_z}{\sqrt{1-w_x^2}} & w_z \end{bmatrix}. \quad (15)$$

By applying the Sarrus rule, we can easily verify that

$$\begin{aligned} \det \boldsymbol{R}_t &= w_y^2 + \frac{w_x^2 w_z^2}{1-w_x^2} + \frac{w_x^2 w_y^2}{1-w_x^2} + w_z^2 \\ &= w_y^2 + w_z^2 + \left(w_y^2 + w_z^2\right) \frac{w_x^2}{w_y^2 + w_z^2} \\ &= w_x^2 + w_y^2 + w_z^2 = 1. \end{aligned}$$

As a last check, it is interesting note the form taken by contact force $\widehat{\boldsymbol{F}}_c$ in the contact frame. Using the transpose $\boldsymbol{R}_t^T$ of the rotation matrix in (15), we obtain

$$\begin{aligned} {}^t\widehat{\boldsymbol{F}}_c = \boldsymbol{R}_t^T \widehat{\boldsymbol{F}}_c &= \boldsymbol{R}_t^T \frac{\widehat{\boldsymbol{F}}_c}{\|\widehat{\boldsymbol{F}}_c\|} \|\widehat{\boldsymbol{F}}_c\| = \boldsymbol{R}_t^T \boldsymbol{w} \|\widehat{\boldsymbol{F}}_c\| \\ &= \begin{bmatrix} \boldsymbol{u}^T \\ \boldsymbol{v}^T \\ \boldsymbol{w}^T \end{bmatrix} \boldsymbol{w} \|\widehat{\boldsymbol{F}}_c\| = \begin{bmatrix} 0 \\ 0 \\ 1 \end{bmatrix} \|\widehat{\boldsymbol{F}}_c\| = \begin{bmatrix} 0 \\ 0 \\ \|\widehat{\boldsymbol{F}}_c\| \end{bmatrix}, \end{aligned}$$

which completely agrees with the contact frame definition, i.e., the contact force $\widehat{\boldsymbol{F}}_c$ is aligned with the $\boldsymbol{z}_t$ axis.

3) $w_x = 0$, i.e., no contact force along $\boldsymbol{x}_0$ direction. Provided that $\|\widehat{\boldsymbol{F}}_c\| \neq 0$, $|w_y|$ and/or $|w_z|$ are non-zero. Thus, the same previous considerations can be made for a different component of $\boldsymbol{w}$, obtaining a different expression for the rotation matrix $\boldsymbol{R}_t$.

IV. Hybrid Force/Velocity Control at the Contact

Consider the robot dynamic model in (5) and the feedback linearization control law

$$\boldsymbol{\tau} = \boldsymbol{M}\boldsymbol{a} + \boldsymbol{n} - \boldsymbol{J}_c^T \widehat{\boldsymbol{F}}_c,$$

which leads, in ideal conditions, to a linear and decoupled system of double integrators $\ddot{\boldsymbol{q}} = \boldsymbol{a}$. With reference to (4), the control input $\boldsymbol{a}$ is chosen as

$$\boldsymbol{a} = \boldsymbol{J}_c^{\#} \boldsymbol{M}_d^{-1} \left(\boldsymbol{R}_t \, \boldsymbol{a}_c + \boldsymbol{M}_d \left(\dot{\boldsymbol{R}}_t \, {}^t\dot{\boldsymbol{x}}_c - \dot{\boldsymbol{J}}_c \dot{\boldsymbol{q}} \right) \right) + \boldsymbol{P}_c \ddot{\boldsymbol{q}}_0, \quad (16)$$

where $\boldsymbol{M}_d = \left(\boldsymbol{J}_c \boldsymbol{M}^{-1} \boldsymbol{J}_c^T \right)^{-1}$ is the natural inertia of the robot at the contact point and $\boldsymbol{a}_c \in \mathbb{R}^3$ is a new auxiliary acceleration input to be chosen so as to control the contact force and the robot motion in two complementary subspaces.

We shall follow a notation similar to the one in [24, Chap. 9]. With the choice

$$\boldsymbol{a}_c = \boldsymbol{S}_f^c \, \ddot{y}_f + \boldsymbol{S}_\nu^c \, \dot{\boldsymbol{\nu}}, \quad (17)$$

a complete decoupling between force control and velocity control can be achieved. Note that, all quantities in (17) are referred to the contact task frame. Moreover, the velocity and acceleration of the contact point along the direction of controlled force are denoted, respectively, by $\dot{y}_f$ and $\ddot{y}_f$[1]. The matrices $\boldsymbol{S}_f^c$ and $\boldsymbol{S}_\nu^c$ are known as *selection matrices* and play in general a fundamental role in the task specification. When expressed in the contact task frame, they are constant and remain consistent with the human-robot contact geometry. In particular, we shall consider a force regulation task along the instantaneous direction of the applied external force, and a velocity tracking control task in the orthogonal plane. For this problem, the dimension of the force controlled subspace is $\lambda = 1$, while the dimension of the velocity controlled subspace is $3 - \lambda = 2$. The matrices $\boldsymbol{S}_f^c$ and $\boldsymbol{S}_\nu^c$ are

$$\boldsymbol{S}_f^c = \begin{bmatrix} 0 \\ 0 \\ 1 \end{bmatrix} \quad \boldsymbol{S}_\nu^c = \begin{bmatrix} 1 & 0 \\ 0 & 1 \\ 0 & 0 \end{bmatrix}. \quad (18)$$

Regulation of the contact force to the desired constant value $F_d > 0$ is obtained by choosing $\ddot{y}_f$ in (17) as

$$\ddot{y}_f = k_f \left(F_d - \|\widehat{\boldsymbol{F}}_c\| \right) - k_{df} \dot{y}_f, \quad (19)$$

where $k_f > 0$ is the force error gain and $k_{df} > 0$ denotes the velocity damping gain in the force controlled direction. The motion dynamics in the force controlled direction is then described as

$$\ddot{y}_f + k_{df} \dot{y}_f = k_f e_f,$$

where $e_f = F_d - \|\widehat{\boldsymbol{F}}_c\|$ is the force regulation error. On the other hand, the desired velocity $\boldsymbol{\nu}_d$ can be achieved by using for $\dot{\boldsymbol{\nu}}$ in (17) the control law

$$\dot{\boldsymbol{\nu}} = \dot{\boldsymbol{\nu}}_d + \boldsymbol{K}_\nu \left(\boldsymbol{\nu}_d - \boldsymbol{\nu} \right) + \boldsymbol{K}_i \int_0^t \left(\boldsymbol{\nu}_d - \boldsymbol{\nu} \right) \boldsymbol{d}s, \quad (20)$$

where $\boldsymbol{K}_\nu > 0$ and $\boldsymbol{K}_i > 0$ are diagonal gain matrices, and

$$\boldsymbol{\nu} = [\boldsymbol{S}_\nu^c]^T \, \boldsymbol{R}_t^T \dot{\boldsymbol{x}}_c = [\boldsymbol{S}_\nu^c]^T \, {}^t\dot{\boldsymbol{x}}_c \in \mathbb{R}^2$$

is the velocity of the contact point projected in the motion subspace. The dynamics of the velocity error is described by

$$\ddot{\boldsymbol{e}}_{\boldsymbol{\nu}} + \boldsymbol{K}_\nu \, \dot{\boldsymbol{e}}_{\boldsymbol{\nu}} + \boldsymbol{K}_i \, \boldsymbol{e}_{\boldsymbol{\nu}} = \boldsymbol{0},$$

with $\boldsymbol{K}_\nu$ and $\boldsymbol{K}_i$ determining the convergence rate of the error $\boldsymbol{e}_{\boldsymbol{\nu}} = \int_0^t \left(\boldsymbol{\nu}_d - \boldsymbol{\nu} \right) \boldsymbol{d}s$ to zero.

Finally, the control input $\boldsymbol{a}$ becomes

$$\begin{aligned} \boldsymbol{a} = \boldsymbol{J}_c^{\#} \boldsymbol{M}_d^{-1} \Big(& \boldsymbol{S}_f (k_f e_f - k_{df} \dot{y}_f) + \boldsymbol{S}_\nu \left(\dot{\boldsymbol{\nu}}_d + \boldsymbol{K}_\nu \dot{\boldsymbol{e}}_{\boldsymbol{\nu}} + \boldsymbol{K}_i \boldsymbol{e}_{\boldsymbol{\nu}} \right) \\ & + \boldsymbol{M}_d \dot{\boldsymbol{R}}_t \, {}^c\dot{\boldsymbol{x}} - \boldsymbol{M}_d \dot{\boldsymbol{J}}_c \dot{\boldsymbol{q}} \Big) + \boldsymbol{P}_c \, \ddot{\boldsymbol{q}}_0, \end{aligned} \quad (21)$$

with matrices $\boldsymbol{S}_f = \boldsymbol{R}_t \boldsymbol{S}_f^c$ and $\boldsymbol{S}_\nu = \boldsymbol{R}_t \boldsymbol{S}_\nu^c$ being time-varying with $\boldsymbol{R}_t$. This time dependence is due to possible changes in the human-robot contact geometry. Without loss of generality, we will suppose that during interaction tasks

[1]We assume that some compliance is present in the force controlled direction, and design the force control loop according to [25]. This is consistent with the fact that the (human) environment is not infinitely stiff.

the human-robot contact type changes sufficiently slow to produce a negligible $\dot{\boldsymbol{R}}_t$. Thus, the resulting control torque $\boldsymbol{\tau}$ becomes

$$\begin{aligned}\boldsymbol{\tau} \;=\; & \boldsymbol{M}\boldsymbol{J}_c^{\#}\boldsymbol{M}_d^{-1}\left(\boldsymbol{S}_f\ddot{y}_f + \boldsymbol{S}_\nu\dot{\boldsymbol{\nu}} - \boldsymbol{M}_d\dot{\boldsymbol{J}}_c\dot{\boldsymbol{q}}\right) \\ & + \boldsymbol{M}\boldsymbol{P}_c\,\ddot{\boldsymbol{q}}_0 + \boldsymbol{n} - \boldsymbol{J}_c^T\widehat{\boldsymbol{F}}_c.\end{aligned} \tag{22}$$

V. Experimental Results

Dynamic interaction experiments between human and robot have been performed using the proposed hybrid control scheme on a KUKA LWR4, using the FRI in torque control mode. The workspace is monitored by a Kinect depth sensor, positioned at about 3.2 m far from the robot. The Kinect captures 640×480 depth images at 30 Hz rate. The entire process of contact force estimation and force/velocity control is executed on an quad-core CPU, with a cycle time of 5 ms.

Since the dimension of the considered task space is $m = 3$ (we are controlling the scalar value of the contact force in one direction and the contact velocity along two other directions in an orthogonal plane), the robot will be redundant for contact tasks that occur on link i, as soon as $i \geq 4$ [14]. In these cases, an extra control action has been considered in the null-space of the contact Jacobian. In particular, the null-space acceleration vector has been chosen in (22) as $\ddot{\boldsymbol{q}}_0 = -\boldsymbol{K}_N\dot{\boldsymbol{q}}$, with $\boldsymbol{K}_N > 0$, in order to bound/damp out self-motions of the arm. Hence, the final control law used to command the robot is

$$\begin{aligned}\boldsymbol{\tau} \;=\; & \boldsymbol{M}\boldsymbol{J}_c^{\#}\boldsymbol{M}_d^{-1}\left(\boldsymbol{S}_f\ddot{y}_f + \boldsymbol{S}_\nu\dot{\boldsymbol{\nu}} - \boldsymbol{M}_d\dot{\boldsymbol{J}}_c\dot{\boldsymbol{q}}\right) \\ & - \boldsymbol{M}\boldsymbol{P}_c\,\boldsymbol{K}_N\dot{\boldsymbol{q}} + \boldsymbol{C}\dot{\boldsymbol{q}} - \boldsymbol{J}_c^T\widehat{\boldsymbol{F}}_c.\end{aligned} \tag{23}$$

The gravity term has been deleted from the commanded user torque, since the KUKA LWR has a built-in gravity compensation.

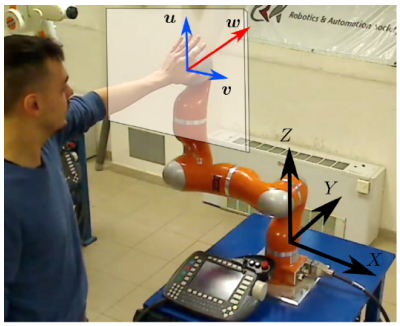

Fig. 2. The set-up of the first hybrid force/velocity control experiment, with the contact frame and the Cartesian reference frame. The motion task is executed on the plane orthogonal to the estimated contact force direction, highlighted in red.

In the first interaction experiment, the human pushes the robot on link $i = 6$. In order to make the following results easier to understand, the human pushes the robot mostly along the Y axis, so that the orthogonal plane can be considered overlapped to the XZ plane, as shown in Fig. 2. The parameters in (19) were set to $k_f = 5.3$, $k_{df} = 18.5$, while the desired value of the contact force was chosen to be $F_d = 15$ N. As for the motion task in the orthogonal plane, the desired velocity has been chosen as $\boldsymbol{\nu}_d = \begin{bmatrix} 0.015 & 0.03 \end{bmatrix}^T$ m/s (with desired acceleration $\dot{\boldsymbol{\nu}}_d = \boldsymbol{0}$). The remaining parameters in (20) and (23) were set to $\boldsymbol{K}_\nu = 60 \cdot \boldsymbol{I}_2$, $\boldsymbol{K}_i = 135 \cdot \boldsymbol{I}_2$, and $\boldsymbol{K}_N = 15 \cdot \boldsymbol{I}_7$, where $\boldsymbol{I}_k$ denotes the $k \times k$ identity matrix.

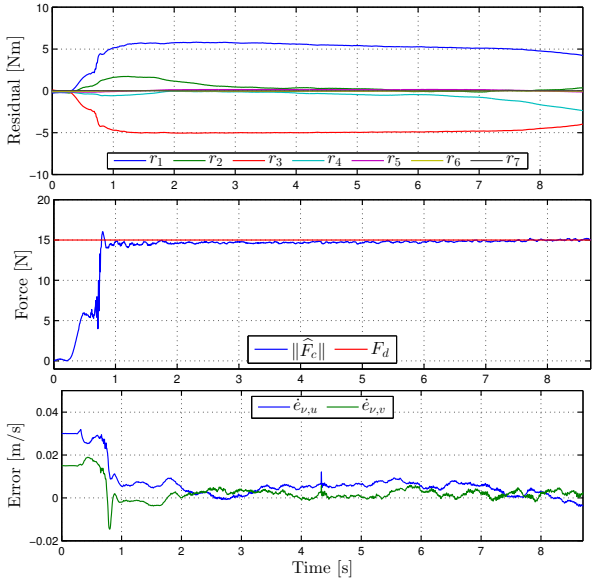

Fig. 3. Hybrid force/velocity control with a constant velocity reference: Residual vector components [top], norm of the estimated contact force [center], and components of the velocity error $\dot{\boldsymbol{e}}_\nu$ [bottom].

Figure 3 shows the behavior of the residual vector $\boldsymbol{r}$, of the norm of the estimated contact force $\|\widehat{\boldsymbol{F}}_c\|$, and of the velocity error $\dot{\boldsymbol{e}}_{\boldsymbol{\nu}} = \boldsymbol{\nu}_d - \boldsymbol{\nu}$. When the human starts pushing on the robot, the robot reacts very quickly in order to regulate the contact force to the desired level. At the same time, the motion task is executed in the corresponding orthogonal subspace. Figure 4(a) shows the motion performed by the contact point $\boldsymbol{x}_c$ in the XZ plane. As expected, it is a straight path with slope $\Delta \simeq \nu_{d,v}/\nu_{d,u} = 2$. Figure 4(b) shows the actual trajectory performed in the XY plane. Note that the contact force along Y remains almost constant, even when the contact point is slightly moving along the Y direction. Moreover, motion and forces along this direction do not perturb the motion task being executed in the orthogonal XZ plane, demonstrating the desired dynamically decoupled behavior. A view of the contact point motion in the 3D Cartesian space is given in Fig. 5.

During the second interaction experiment, the human is pushing against link $i = 7$ of the robot. As in the first experiment, the robot is being pushed mainly along one of the Cartesian directions, now X, so that the new orthogonal plane can be assumed to be parallel to the YZ plane, as shown in Fig. 6. In this experiment, the desired velocity $\boldsymbol{\nu}_d$ and acceleration $\dot{\boldsymbol{\nu}}_d$ vector have been chosen in order to perform at constant speed a circle with radius $\rho = 0.12$ m in the motion subspace. They can be written as

$$\boldsymbol{\nu}_d = \begin{bmatrix} \omega\rho\,\sin\omega t \\ \omega\rho\,\cos\omega t \end{bmatrix} \qquad \dot{\boldsymbol{\nu}}_d = \begin{bmatrix} \omega^2\rho\,\cos\omega t \\ -\omega^2\rho\,\sin\omega t \end{bmatrix}, \tag{24}$$

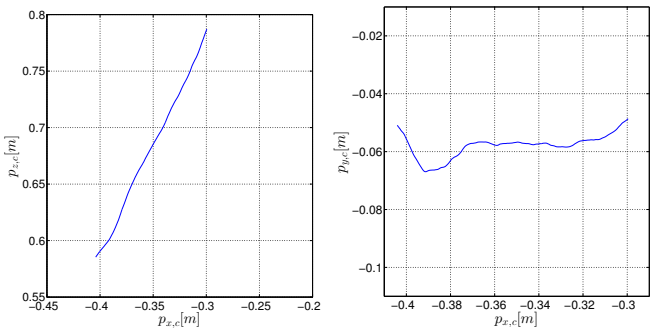

(a) (b)

Fig. 4. Trajectory performed during the first interaction task by the contact point $\boldsymbol{x}_c$ in the XZ plane [left] and in the XY plane [right], which is also the view from the top.

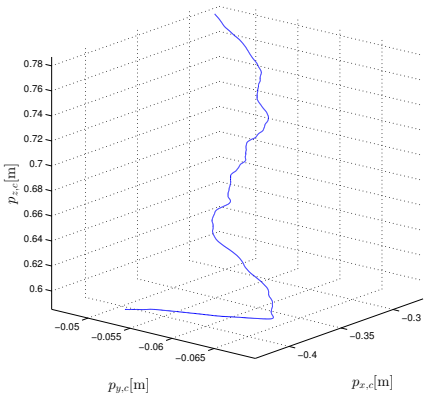

Fig. 5. View of the trajectory performed by the contact point $\boldsymbol{x}_c$ in the 3D Cartesian space, with a constant velocity reference.

with angular frequency $\omega = 2\pi/T \simeq 0.628$, providing a period of $T = 10$ s. The hybrid scheme (23) was used again, with the parameters in (19) being set to $k_f = 5.8$ and $k_{df} = 18.5$ and desired contact force to $F_d = 15$ N. The parameters in (20) were set to $\boldsymbol{K}_\nu = 42 \cdot \boldsymbol{I}_2$ and $\boldsymbol{K}_i = 155 \cdot \boldsymbol{I}_2$. Lastly, the null space gain was left unchanged, i.e., $\boldsymbol{K}_N = 15 \cdot \boldsymbol{I}_7$.

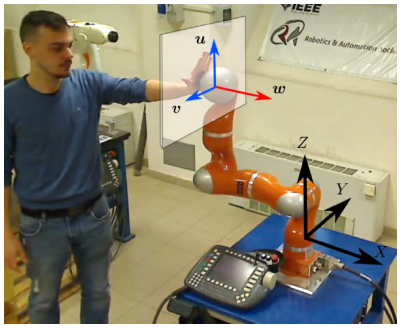

Fig. 6. The set-up of the second hybrid force/velocity control experiment, with the contact frame and the Cartesian reference frame. A circular motion task is executed on the plane orthogonal to the estimated contact force direction, highlighted in red.

As before, Figure 7 shows the behavior of the residual vector $\boldsymbol{r}$, of the norm of the estimated contact force $\|\widehat{\boldsymbol{F}}_c\|$, and of the velocity error $\dot{\boldsymbol{e}}_{\boldsymbol{\nu}}$. Again, the robot is able to regulate almost immediately the contact force to the desired level, as soon as the human pushes on link 7 (the instant of contact is identified by the residuals starting to drift away from zero). The motion task is independently performed in the orthogonal subspace for 40 s, so that about 4 complete circles are traced. The presence of multiple, almost overlapping circular paths in Fig. 8(a) confirms the effectiveness of the proposed hybrid control law. Figure 8(b) shows the path executed in the XY plane. As expected, even if the contact point is moving along X direction, the contact force remains almost constant. The actual motion of the contact point in the 3D Cartesian space, forming a spiral, is shown in Fig. 9.

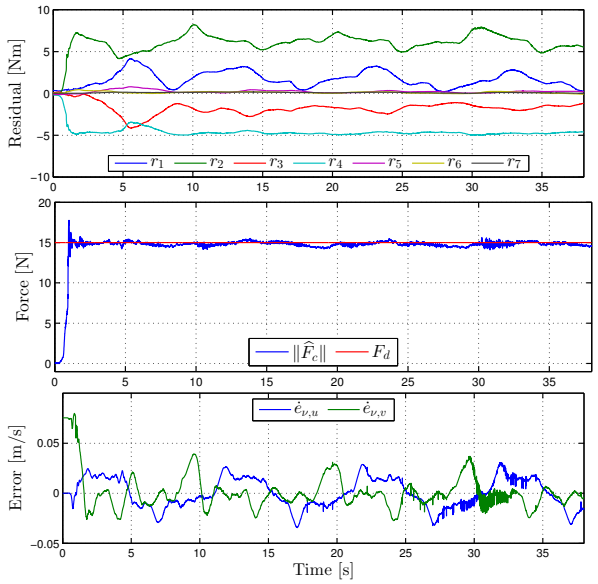

Fig. 7. Hybrid force/velocity control with a sinusoidal velocity reference: Residual vector components [top], norm of the estimated contact force [center], and components of the velocity error $\dot{\boldsymbol{e}}_{\nu}$ [bottom].

The above two experiments can be seen in the accompanying video clip. We note finally that in all cases the hybrid force/velocity controller has been switched on only when the norm of the estimated force has become larger than 5 N. On the other hand, when the contact force estimate suddenly falls below 50% of the desired value (here, below 7.5 N), the controller recognizes that the human has (intentionally) lost contact with the robot, and thus the robot motion is stopped right away.

VI. Conclusion

We have introduced and implemented a generalized hybrid force/velocity control scheme realized at the contact point, without the explicit need of a force sensor and relying on a fast estimation of the contact force. The human-robot contact geometry defines a task frame in which both regulation of the contact force to a desired value along the approach direction and execution of a motion with desired velocity in the corresponding orthogonal plane are feasible. Satisfactory performance has been obtained during different human-robot interaction experiments performed with a KUKA LWR robot manipulator. This approach, together with our previous work

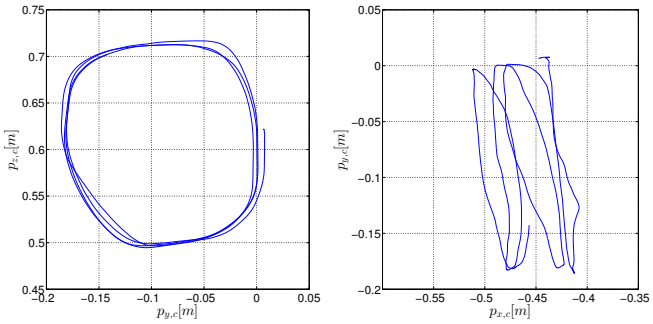

(a) (b)

Fig. 8. Trajectory performed during the second interaction task by the contact point $\boldsymbol{x}_c$ in the YZ plane [left] and in XY plane [right], which is also the view from the top.

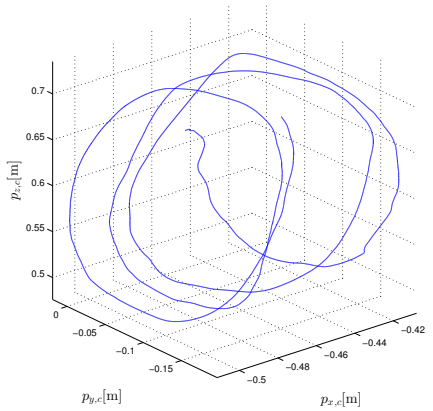

Fig. 9. View of the trajectory performed by the contact point $\boldsymbol{x}_c$ in the 3D Cartesian space, with a sinusoidal velocity reference.

on the generalization of classical admittance, impedance, and direct force control schemes to a generic contact location identified on line, extends the portfolio of available controllers for physical human-robot interactions tasks.

REFERENCES

[1] A. De Santis, B. Siciliano, A. De Luca, and A. Bicchi, "An atlas of physical human-robot interaction," *Mechanism and Machine Theory*, vol. 43, no. 3, pp. 253–270, 2008.

[2] SAPHARI. Safe and Autonomous Physical Human-Aware Robot Interaction. [Online]. Available: www.saphari.eu

[3] A. De Luca and F. Flacco, "Integrated control for pHRI: Collision avoidance, detection, reaction and collaboration," in *Proc. IEEE Int. Conf. on Biomedical Robotics and Biomechatronics*, 2012, pp. 288–295.

[4] ISO 10218-1-2011. Robots and robotic devices – Safety requirements for industrial robots. Part 1: Robots; Part 2: Robot systems and integration. [Online]. Available: http://www.iso.org (since July 1, 2011).

[5] ISO TS 15066:2016. Robots and robotic devices – Collaborative robots. [Online]. Available: http://www.iso.org (since February 15, 2016).

[6] A. De Luca and R. Mattone, "Sensorless robot collision detection and hybrid force/motion control," in *Proc. IEEE Int. Conf. on Robotics and Automation*, 2005, pp. 1011–1016.

[7] A. De Luca, A. Albu-Schäffer, S. Haddadin, and G. Hirzinger, "Collision detection and safe reaction with the DLR-III lightweight robot arm," in *Proc. IEEE/RSJ Int. Conf. on Intelligent Robots and Systems*, 2006, pp. 1623–1630.

[8] S. Haddadin, A. Albu-Schäffer, A. De Luca, and G. Hirzinger, "Collision detection and reaction: A contribution to safe physical human-robot interaction," in *Proc. IEEE/RSJ Int. Conf. on Intelligent Robots and Systems*, 2008, pp. 3356–3363.

[9] F. Flacco, T. Kröger, A. De Luca, and O. Khatib, "A depth space approach for evaluating distance to objects – with application to human-robot collision avoidance," *J. of Intelligent & Robotic Systems*, vol. 80, Suppl. 1, pp. 7–22, 2015.

[10] F. Flacco and A. De Luca, "Real-time computation of distance to dynamic obstacles with multiple depth sensors," *IEEE Robotics and Automation Lett.*, vol. 1, no. 1, 2016.

[11] L. Lucignano, F. Cutugno, S. Rossi, and A. Finzi, "A dialogue system for multimodal human-robot interaction," in *Proc. 15th ACM Int. Conf. on Multimodal Interaction*, 2013, pp. 197–204.

[12] S. Iengo, S. Rossi, M. Staffa, and A. Finzi, "Continuous gesture recognition for flexible human-robot interaction," in *Proc. IEEE Int. Conf. on Robotics and Automation*, 2014, pp. 4863–4868.

[13] A. Cirillo, F. Ficuciello, C. Natale, and S. Pirozzi, "A conformable force/tactile skin for physical human-robot interaction," *IEEE Robotics and Automation Letters*, vol. 1, no. 1, pp. 41–48, 2016.

[14] E. Magrini, F. Flacco, and A. De Luca, "Estimation of contact forces using a virtual force sensor," in *Proc. IEEE/RSJ Int. Conf. on Intelligent Robots and Systems*, 2014, pp. 2126–2133.

[15] F. Ficuciello, L. Villani, and B. Siciliano, "Variable impedance control of redundant manipulators for intuitive human-robot physical interaction," *IEEE Trans. on Robotics*, vol. 31, no. 4, pp. 850–863, 2015.

[16] E. Magrini, F. Flacco, and A. De Luca, "Control of generalized contact motion and force in physical human-robot interaction," in *Proc. IEEE Int. Conf. on Robotics and Automation*, 2015, pp. 2298–2304.

[17] E. Magrini, "Estimation of Contact Forces and Interaction Control in Human-Robot Collaboration Tasks," Ph.D. dissertation, DIAG, Sapienza Università di Roma, May 2016.

[18] M. T. Mason, "Compliance and force control for computer controlled manipulators," *IEEE Trans. on Systems, Man, and Cybernetics*, vol. 11, no. 6, pp. 418–432, 1981.

[19] M. H. Raibert and J. J. Craig, "Hybrid position/force control of manipulators," *ASME J. Dynamic Systems, Measurement, and Control*, vol. 103, no. 2, pp. 126–133, 1981.

[20] W. D. Fisher and M. S. Mujtaba, "Hybrid position/force control: A correct formulation," *Int. J. of Robotics Research*, vol. 11, no. 4, pp. 299–311, 1992.

[21] O. Khatib, "A unified approach for motion and force control of robot manipulators: The operational space formulation," *IEEE Trans. on Robotics and Automation*, vol. 3, no. 1, pp. 43–53, 1987.

[22] T. Yoshikawa, "Dynamic hybrid position/force control of manipulators — Description of hand constraints and calculation of joint driving force," *IEEE J. of Robotics and Automation*, vol. 3, no. 5, pp. 386–392, 1987.

[23] A. De Luca, C. Manes, and G. Ulivi, "Robust hybrid dynamic control of robot arms," in *Proc. 28th IEEE Conf. on Decision and Control,*, 1989, pp. 2641–2646.

[24] B. Siciliano, L. Sciavicco, L. Villani, and G. Oriolo, *Robotics: Modeling, Planning and Control*, 3rd ed. London: Springer, 2008.

[25] A. De Luca, C. Manes, and F. Nicolò, "A task space decoupling approach to hybrid control of manipulators," in *Proc. 2nd IFAC Symp. on Robot Control*, 1988, pp. 157–162.